6280 *Chem. Mater.* **2010,** *22,* 6280–6290
DOI:10.1021/cm101961g

CHEMISTRY OF MATERIALS
Article

# Geometric Control and Intense Plasmon Resonances of Colloidal Truncated Triangular Copper Nanoplates in Nonionic Microemulsions Containing Tetrabutylammonium Hydroxide

Young S. Park and Hee K. Chae*

*Department of Chemistry Education, Seoul National University, Seoul, 151-748, Korea*

*Received July 15, 2010. Revised Manuscript Received October 2, 2010*

Geometric control of copper nanoparticles was attempted with nonionic microemulsions containing tetrabutylammonium hydroxide (TBAOH). By using copper(II) salts as precursors, metallic anisotropic Cu nanoparticles were obtained via a two-step chemical reaction. Corresponding plasmon resonances were monitored under differing reaction conditions. The effect of TBAOH and Cu precursor on the resulting geometries was examined so that the anisotropic morphologies of Cu nanoparticles could be confirmed as evolving under the controlled condition where cupric hydroxides formed predominantly as intermediates. Distinguishable optical spectra dependent upon the geometries of nanoparticles were obtained, and narrow and intense plasmon resonances centered within the range of 585−590 nm were observed from truncated triangular Cu nanoplates with optimum aspect ratios. In addition, the controlled reactions were processed in another two microemulsions by using nonionic surfactants with different lengths of polyoxyethylene groups. Finally, electrodynamics calculations were used to further explain the spectral changes with an increase in the geometric anisotropy of Cu nanoparticles.

## Introduction

An interesting optical response of nanostructured noble metals arises from the coherent collective oscillation of free electrons when electromagnetic irradiations are applied, and is referred to as localized surface plasmon resonance (LSPR).[1−3] Over recent years, LSPRs of metallic nanoparticles including Au and Ag have received intense attention for their opto-physical value as novel optical phenomena[3] and their promising use for sensitive optical sensing,[4] cancer therapeutics,[5] and surface-enhanced Raman spectroscopy.[6] Because the LSPRs are highly sensitive to the size, geometry, composition of metallic nanostructures, and surrounding medium, as well as interparticle spacing,[2,7−10] their manipulation has been pursued by controlling such parameters. In particular, geometric control has been a fascinating route for manipulating the optical response of metallic nanoparticles, increasing the diversity of geometry-dependent LSPRs in terms of spectral ranges and line shapes. Additionally, a good agreement between experimental measurements and theoretical predictions of optical response for the certain nanostructured geometric targets should be allowed on the basis of effective control of geometries.[2,11]

Observations of characteristic geometry-dependent LSPRs of Cu nanoparticles have been made by tailoring geometries, and manipulating their dimensions has resulted in a remarkable variation in LSPRs.[12−15] These have been discussed through particular preparation methods of Cu particles with different geometries. LSPRs have been represented as broad double bands observed from isotropic nanoshells surrounding silica particle cores.[12] Anisotropic particle arrays deposited on hard substrates with a certain orientation also showed characteristic dipolar plasmon resonances. Transverse dipolar LSPR peaks were displayed from parallel nanowires,[13] and single intense dipolar plasmon LSPR peaks were

*Corresponding author. E-mail: hkchae1@snu.ac.kr.

(1) Jain, P. K.; Huang, X; El-Sayed, I. H.; El-Sayed, M. A. *Acc. Chem. Res.* **2008**, *41*, 1578–1586 and references therein. .
(2) Kelly, K. L.; Coronado, E.; Zhao, L. L.; Schatz, G. C. *J. Phys. Chem. B* **2003**, *107*, 668–677.
(3) Wang, H.; Brandl, D. W.; Nordlander, P.; Halas, N. J. *Acc. Chem. Res.* **2007**, *40*, 53–62.
(4) Reynolds, R. A.; Mirkin, C. A.; Letsinger, R. L. *J. Am. Chem. Soc.* **2000**, *122*, 3795–3796.
(5) Au, L.; Zheng, D.; Zhou, F.; Li, Z. Y.; Li, X.; Xia, Y. *ACS Nano* **2008**, *2*, 1645–1652.
(6) Mulvaney, S. P; Musick, M. D.; Keating, C. D.; Natan, M. J. *Langmuir* **2003**, *19*, 4784–4790.
(7) Njoki, P. N.; Lim, I.-I. S.; Mott, D.; Park, H.-Y.; Khan, B.; Mishra, S.; Sujakumar, R.; Luo, J.; Zhong, C.-J. *J. Phys. Chem. C* **2007**, *111*, 14664–14669.
(8) Chen, H; Kou, X.; Yang, Z.; Ni, W.; Wang, J. *Langmuir* **2008**, *24*, 5233–5237.
(9) Kim, S.; Kim, S. K.; Park, S. *J. Am. Chem. Soc.* **2009**, *131*, 8380–8381.
(10) Jensen, T. R.; Duval, M. L.; Kelly, K. L.; Lazarides, A. A.; Schatz, G. C; Van Duyne, R. P. *J. Phys. Chem. B* **1999**, *103*, 9846–9853.
(11) Liz-Marzán, L. M. *Langmuir* **2006**, *22*, 32–41.
(12) Wang, H; Tam, F.; Grady, N. K.; Halas, N. J. *J. Phys. Chem. B* **2005**, *109*, 18218–18222.
(13) Zong, R. L.; Zhou, J.; Li, B.; Fu, M.; Shi, S. K; Li, L. T. *J. Chem. Phys.* **2005**, *123*, 094710.
(14) Chan, G. H.; Zhao, J.; Hicks, E. M.; Schatz, G. C.; Van Duyne, R. P. *Nano Lett.* **2007**, *7*, 1947–1952.
(15) Salzemann, C.; Brioude, A.; Pileni, M.-P. *J. Phys. Chem. B* **2006**, *110*, 7208–7212.


Published on Web 11/11/2010

observed from triangular particles[14] in localized areas where Cu deposition was performed. Such geometry-dependent LSPRs could be remarkably tuned by the control of particle size[12−14] and, in particular, oriented one-dimensional nanowires showed strong dependence of LSPRs upon the angles of light incidence.[14]

The LSPRs of collections of anisotropic Cu nanodisks, isotropic nanospheres, and nanocubes have been investigated by wet-chemical methods using anionic micellar templates. Distinctive plasmon resonances have been measured by controlling the relative proportions of nanodisks and nanospheres.[15,16] The spectral change of LSPRs as the proportion of anisotropic particles increased up to about 60% of Cu colloids was explained by comparing experimental spectra with calculated optical results obtained by taking into account the experimentally determined proportions of nanodisks. Specifically, a red-shifted broad plasmon resonance was measured from a Cu colloid containing the highest proportion of Cu nanodisks.[15] The experimental spectra of the anisotropic particles were, however, rather different from calculated spectra because of the large shape distribution of the whole colloid.

To clarify an influence of nanoparticle aspect ratios on the optical spectra of colloidal anisotropic Cu nanoparticles, we proposed nonionic W-in-O microemulsion strategies for the synthesis and geometric control of colloidal truncated triangular nanoplates in the presence of ionic stabilizers such as tetrabutylammoniums (TBAs) and alkyl carboxylates in water phases. By utilizing W-in-O microemulsions as microreactors, the anisotropic control of Cu nanoparticles after the reduction of cupric hydroxide would be conducted by ionic stabilizers such TBA alkyl carboxylates released after the formation of cupric hydroxide. $TBA^+$ ions have been known to form micelles or vesicles with alkyl carboxylates in water phase.[17,18] Plus, the ability of $TBA^+$ ions to solubilize and transfer hydrophobic alkyl carboxylates by forming micelles into aqueous phase was expected to give rise to ionic stabilization of TBA salts on metal surfaces. In particular, $TBA^+$ ions were also reported to be superior to that of quaternary ammonium cations with shorter chains, such as ethyl or methyl groups.[19] Our previous study indicated the insufficient anisotropic control of Cu nanoparticles into anisotropic morphologies occurred yielding a large amount (~40%) of spherical particles when using tetraethylammonium cations.

On the basis of the expectation of improved ionic stabilization on metallic Cu nanoparticles by more hydrophobic tetrabutylammonium alkyl carboxylates in the aqueous solution, we examined the effect of reactant concentrations on the aspect ratios of obtained Cu nanoparticles, and found that anisotropic control of Cu nanoparticles into truncated triangular plates can be induced in the nonionic microemulsions by monitoring distinctive plasmon resonances of anisotropic Cu nanoparticles with optimum aspect ratios. In addition, the controlled reactions yielding anisotropic particles were processed in another two nonionic microemulsions to confirm the similarity in the production of anisotropic particles and evolution of LSPRs under the same reaction condition. The spectral change of LSPRs with increasing geometric anisotropy of Cu particles was also investigated by comparing theoretically calculated results to experimental LSPRs of Cu nanoparticles in terms of spectral shift and fluctuation in intensity.

## Experimental Section

**Chemicals.** Nonionic surfactants such as Igepal CO-520 (NP-5), CO-720 (NP-12) and *n*-hexyl alcohol, tetrabutylammonium hydroxide solution (TBAOH, 40 wt %), hydrazine monohydrate ($N_2H_4 \cdot H_2O$), and copper(II) 2-ethyl hexanoate ($Cu(EH)_2$) were received from Aldrich corporation. Tergitol NP-9 (NP-9) was purchased from Fluka. Cyclohexane (CHA, J. T. Baker) and deionized water (18.2 MΩ cm) were also required to compose microemulsions. The chemicals were used without further purification. $Cu(EH)_2$ was dissolved in cyclohexene (CHE), and $N_2H_4 \cdot H_2O$ in water to prepare 8−12 M aqueous solutions before use.

**Synthesis.** Nonionic surfactant solutions (A) that contain NP-9 in CHA (2.6 mmol/18 mL) were separated into two portions by transferring 8-mL aliquots of each NP-9 solution to another vial (B). The volumes of TBAOH solutions and additional water were dispersed in A under agitation and the volumes of reducing agent $N_2H_4$ (0.72−1.44 mmol) were dispersed in B, respectively. After the two emulsions were stabilized, the 0.5−1.5 mL of $Cu(EH)_2$ solutions was added to the A, waiting 15 min for reaction. The concentration of TBAOH was adjusted by varying the added volume of water, while maintaining the fixed water phase volume. The $[TBAOH]/[Cu(EH)_2]$ was adjusted from 2.0 to 4.7. The reduction was initiated by mixing two emulsions (A and B) under moderate agitation, and the reaction progressed for 6−8 h at room temperature. In NP-5 and NP-12 microemulsions, identical processes were available for the synthesis of Cu truncated triangular nanoplates. The 5 mmol of NP-5 was needed to stabilize microemulsion systems, and the 1.8 mmol of NP-12 was used with *n*-hexyl alcohol (7.3 mmol) for stabilization.

**Characterization.** The Fourier transform infrared (FT-IR) spectra (PerkinElmer, Spectro 2000 Explorer) of $Cu(EH)_2$ and $Cu(OH)_2$ were recorded from the isolated solids after washed with ethanol and diethyl ether, respectively. Powder X-ray diffraction (PXRD) patterns were collected through X-ray diffractometer (MAC Science, M18XHF-SRA). Then the LSPRs of resulting Cu nanoparticles in nonionic microemulsions were measured by a UV−vis spectrometer (Varian, Cary). The overall geometries were characterized by a high-resolution TEM (HRTEM, JEOL, JEM 2010) equipped with CCD cameras from the samples on copper grids, and selected area electron diffraction (SAED) patterns were taken by using the HRTEM.

**Electrodynamics Calculations.** The discrete dipolar approximation (DDA) has been accepted as one of the powerful numerical methods useful for investigating the scattering and absorption of given Cu targets with arbitrary geometries.

(16) Salzemann, C.; Lisiecki, I; Urban, J.; Pileni, M. -P. *Langmuir* **2004**, *20*, 11772–11777.
(17) Zana, R.; Schmidt, J.; Talmon, Y. *Langmuir* **2005**, *21*, 11628–11636.
(18) Ruiz, F.-J.; Rubio, S.; Pérez-Bendito, D. *Anal. Chem.* **2006**, *78*, 7229–7239.
(19) Lin, B; McCormick, A. V.; Davis, H. T.; Strey, R. *J. Colloid Interface Sci.* **2005**, *291*, 543–549.

**Scheme 1. Two-Step Reaction Processed in Nonionic W-in-O Microemulsions by Mixing Two Microemulsions**

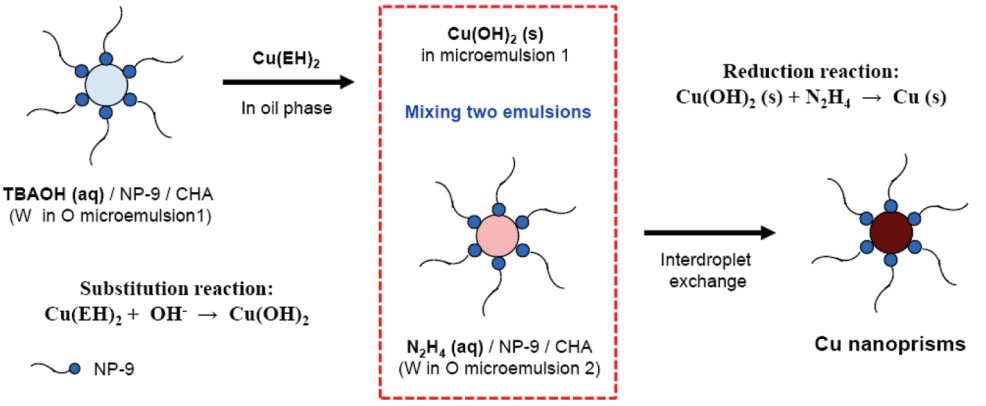


The DDA calculations were carried out utilizing the implementation developed by Draine and Platau.[21,22] The number of dipoles were established higher than 21 000 in all calculations.

## Results and Discussion

**Synthesis of Anisotropic Cu Nanoparticles via As-Prepared $Cu(OH)_2$.** Two-step chemical reactions are involved in the nonionic reverse microemulsion synthesis. One step is the reaction of copper(II) alkyl carboxylates with hydroxide ions, and the other is the reduction of as-prepared cupric hydroxides into copper nanoparticles. W-in-O microemulsions served as microreactors to confine the resulting size of colloidal Cu particles to below 100 nm. Cu(II) alkyl carboxylates added through a continuous oil phase could approach the dispersed water phase containing TBAOH in the microreactors; they readily reacted with hydroxide ions, releasing alkyl carboxylate anions. Resulting Cu(II) species deposited at the interface of the two phases were introduced to the following reduction reactions.

Additional emulsions containing hydrazine aqueous phase are required for the second reduction step, which proceeded by mixing two emulsions. Two chemical routes can be suggested as follows, and the schematic representation is provided in Scheme 1.

$$Cu(EH)_2 + 2TBA^+ + 2OH^- \rightarrow Cu(OH)_2 + 2TBA^+ + 2EH^- \quad (1)$$

$$Cu(OH)_2 + 1/2N_2H_4 \rightarrow \rightarrow Cu + 2H_2O + 1/2N_2\uparrow \quad (2)$$

In reaction 1, the formation of blue or greenish-blue solids was observed in alkaline solutions that were adjusted by the concentration of TBAOH. The substitution of 2-ethyl hexanoates by free hydroxide ions occurs, yielding copper hydroxides that are blue or blue-green gels or powders in water as shown in eq 1. But it is complicated to clarify the products of the first reaction in detail when the resulting solutions bear different adjusted pH values because of the low stability of copper hydroxide under alkaline conditions. It is noted in the present work that the synthesis of truncated triangular Cu nanoplates was carried out when the $R$, the molar ratio of [TBAOH]/[$Cu(EH)_2$], was kept at 2.0 (see the following sections). The insoluble solid products obtained when $R = 2.0$ could be characterized.

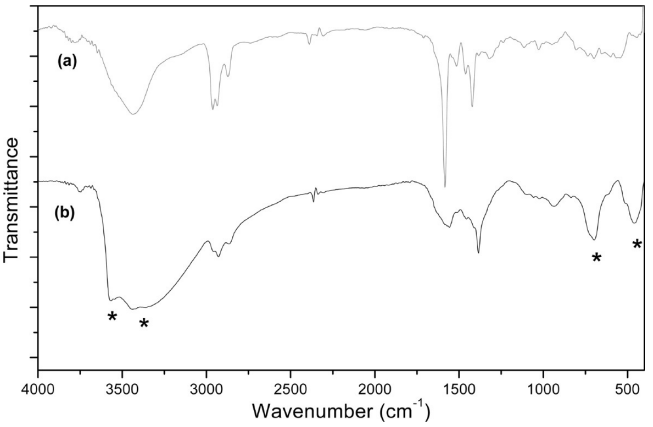


**Figure 1.** FT-IR spectra of (a) Cu(II) 2-ethyl hexanoates and (b) isolated $Cu(OH)_2$ products. The absorption peaks attributed to the $Cu(OH)_2$ are indicated by the asterisks.

Figure 1 shows FT-IR spectra recorded from the $Cu(EH)_2$ precursors and isolated products after alkaline treatment. After reaction 1, the substitution reaction is indicated by the apparent disappearance of a strong stretching vibration peak arising from the coordinated 2-ethylhexnoate anions at 1583 $cm^{-1}$, accompanied by the production of $Cu(OH)_2$ species. An absorption peak at 3565 $cm^{-1}$ and a broad band around 3400 $cm^{-1}$ can be assigned to water-bounded hydroxyl ions of copper hydroxide, and additional two peaks at 698 and 460 $cm^{-1}$ are caused by vibrations of Cu−O and Cu−O−H groups.[23,24] Other peaks arose from $TBA^+$ ions and residual ethyl hexanoate anions.

The predominant production of copper hydroxide obtained at $R = 2.0$ was supported by an X-ray diffraction pattern (see Figure 2). All the reflections of copper hydroxides were indexed to the orthorhombic $Cu(OH)_2$,

(20) Park, Y. S.; Chae, H. K. *J. Nanosci. Nanotechnol.* **2010**, *10*, 383–387.
(21) Draine, B. T.; Flatau, P. J. *J. Opt. Soc. Am. A* **1994**, *11*, 1491–1499.
(22) Draine, B. T.; Flatau, P. J. *Program DDSCAT*; Scripps Institute of Oceanography: La Jolla, CA.
(23) Park, S.-H.; Kim, H. J. *J. Am. Chem. Soc.* **2004**, *126*, 14368–14369.
(24) Liu, N.; Wu, D.; Wu, H.; Luo, F.; Chen, J. *Solid State Sci.* **2008**, *10*, 1049–1055.

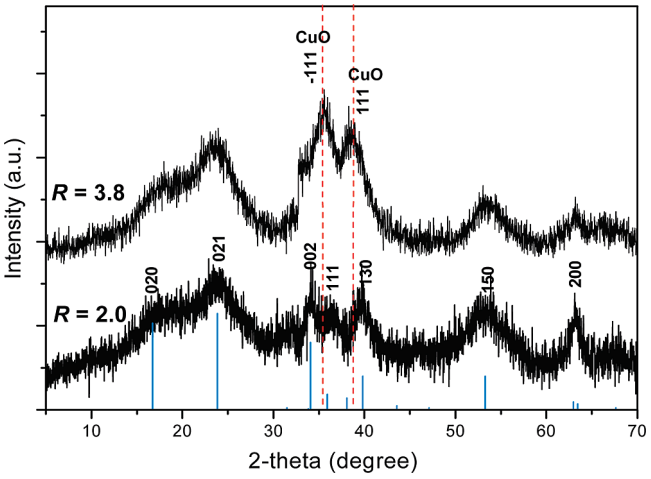


**Figure 2.** PXRD patterns of isolated products obtained after the reaction between TBAOH and $Cu(EH)_2$ at different $R$ values. $R$ indicates the molar ratio of [TBAOH]/[$Cu(EH)_2$].

in agreement with JCPDS 13−0420 and as-prepared $Cu(OH)_2$ from $Cu_2(OH)_3NO_3$.[23] The interfacial formation of $Cu(OH)_2$ nanowires between the immiscible macroscopic phases was also found in previous studies,[24,25] and the high broadness of diffraction patterns would arise from the small sizes of grains formed at the microscopic interface in the discontinuous water phase of microemulsion microreactors. In addition, the partial production of black solids, CuO, at the interface could not be excluded when the concentration of TBAOH was raised to more than twice as much as the concentration of Cu ions. The similar production of CuO took place at the interface of immiscible macroscopic phases when hydroxide ions increased relative to the Cu(II) ions.[25] The XRD pattern of the black precipitate obtained when $R$ = 3.8 in Figure 2 shows intense diffracted peaks that can be exactly assigned to monoclinic CuO (JCPDS 41−0254) through the gradual dehydration of $Cu(OH)_2$.

In reaction 2, the reduction of as-prepared $Cu(OH)_2$ into metallic Cu solids occurred gradually through the inter-droplet dynamic exchange of two water phases containing Cu(II) species and hydrazine. Slow reduction processes prevent the intermediates from being rapidly reduced to too large and irregular Cu particles, but it required quite an excessive amount of $N_2H_4$, which is higher than Cu(II) contents by a factor of 27 in typical syntheses, to maintain a sufficient reduction rate that leads to Cu(0) production. The hydrazine reduction of $Cu(OH)_2$ did not immediately appear to yield Cu particles even with an excessive amount of hydrazine, which was evident through characteristic LSPRs. Figure 3A shows that appearance of copper metallic species by reduction of as-prepared $Cu(OH)_2$ is dependent upon $R$. At $R$ below 2.0, large Cu particle precipitates were deposited at the bottom of glassware, losing colloidal stability through the rapid reduction of Cu(II) species. At $R$ above 2.0, colloidal Cu nanoparticle formation was commonly evident through corresponding LSPRs via the intermediate period which was prolonged for about 2 h; at the intermediate stage only a continuously increasing absorption was observed

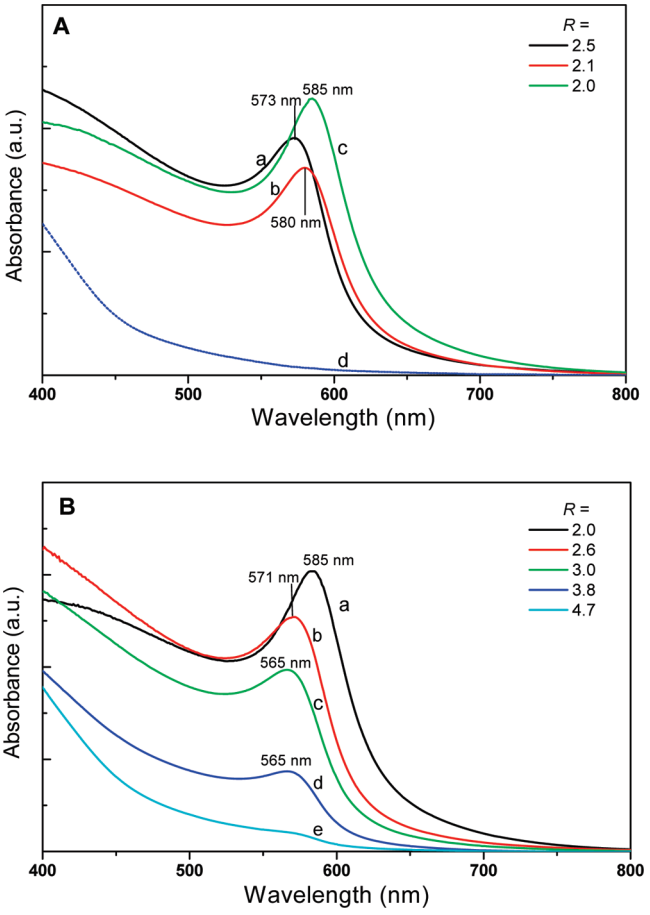


**Figure 3.** (A) UV−vis absorption spectra a−c showing characteristic LSPR peaks recorded from Cu nanoparticles in microemulsions with an increase in the concentration of $Cu(EH)_2$. Spectrum d was recorded before the growth into Cu nanoparticles during reduction of copper hydroxides. (B) UV−vis spectra a−e with an increase in the concentration of TBAOH. Figures indicate the maximum wavelengths ($\lambda_{max}$) of plasmon resonance peaks at different $R$ = [TBAOH]/[$Cu(EH)_2$].

over the visible range, without any plasmon peak within 500 - 600 nm (spectrum d in Figure 3A). A similar optical profile was found from the small Cu nanoparticles with the size of a few nanometers.[26] It is not easy to ascertain the composition of intermediate products, because the low stability of Cu nanoparticles against oxidation causes rapid conversion of Cu to $Cu_2O$. Such a lack of a LSPR peak was also observed from the absorption spectra of $Cu_2O$ nanoparticles.[27] But in this microemulsion synthesis, hydrazine served as a successful reducing agent for the conversion of Cu(II) solids into Cu(0), and consequently, the formation of Cu particles could be detected by plasmon resonance peaks as shown in Figure 3A. The formation of Cu nanoparticles via hydrazine reduction of Cu(II) species soluble in organic solvents were found in previous literatures.[28,29] The similar observation of characteristic LSPRs were made from

(25) Song, X.; Sun, S.; Zhang, W.; Yu, H.; Fan, W. *J. Phys. Chem. B* **2004**, *108*, 5200–5205.
(26) Brege, J. J.; Hamilton, C. E.; Crouse, C. A.; Barron, A. R. *Nano Lett.* **2009**, *9*, 2239–2242.
(27) Chen, Q.; Shen, X.; Gao, H. *J. Colloid Interface Sci.* **2007**, *308*, 491–499.
(28) Curtis, A. C.; Duff, D. G.; Edwards, P. P.; Jefferson, D. A.; Johnson, B. F. G.; Kirkland, A. I.; Wallace, A. S. *Angew. Chem., Int. Ed.* **1988**, *27*, 1530–1533.
(29) Pastoriza-Santos, I.; Sánchez-Iglesias, A.; Rodríguez-González, B.; Liz-Marzán, L. M. *Small* **2009**, *4*, 440–443.

anisotropic Cu nanoparticles with the size of several tens of nanometers.

In addition, when hydroxide ions from TBAOH were consumed during reduction steps (eq 2), 2-ethyl hexanoate ions relatively prevailed and could serve as counterions of $TBA^+$ ions at the expense of hydroxide ions. It was obviously confirmed in previous studies that alkyl carboxylates could be soluble and associated with $TBA^+$ ions to form micellar aggregates in aqueous phase.[17−19] The substitution reaction of $Cu(EH)_2$ with $OH^-$ in eq 1 enables the ethyl hexanoate to pair with $TBA^+$ to form micellar aggregates and to bring the TBA salts in close proximity to the Cu(0) clusters produced during the following reduction reaction below submicrometer ranges in microemulsions.

**Change in Optical Response of Cu Nanoparticles by Regulating the Reactant Molar Ratios.** Once Cu nanoparticles are formed in nonionic microemulsions, the color of the mixtures abruptly turns red or dark red. The Cu nanoparticle formation was monitored through UV−vis spectroscopy. The characteristic LSPR peaks emerged along with the production of Cu nanoparticles. Figure 3 shows the absorption spectra of as-prepared Cu nanoparticles in NP-9 microemulsions under the control of reactant concentrations, and a remarkable dependence of the optical response on reactants such as TBAOH and $Cu(EH)_2$ is observed.

First, the absorption profiles of nanoparticles were strongly affected by the amount of $Cu(EH)_2$, as shown in Figure 3A. By increasing the concentration of $Cu(EH)_2$ under the fixed amount of TBAOH and hydrazine, $R$ values could be decreased. As the $R$ value decreased from 2.5 to 2.0, the maximum wavelength ($\lambda_{max}$) of LSPR peaks was red-shifted from 573 to 585 nm. The regulation of $R$ values also gave rise to a change in line shape of absorption spectra. But further spectral changes were not found with $R$ values higher than 2.5, and reduction process when $R$ is below 2.0 yielded large precipitates losing colloidal stability, rather than Cu colloids. The stoichiometric excess of $Cu(EH)_2$ on completion of $Cu(OH)_2$ after reaction 1 manipulates the reduction routes (reaction 2) by involving the direct hydrazine reduction of remaining $Cu(EH)_2$ precursors. Preliminary experiments to examines the direct reduction of $Cu(EH)_2$ precursors without substitution with TBAOH also resulted in similar production of precipitates, without undergoing the intermediate stage as described in a previous section.

Second, the concentration of TBAOH can also influence the optical response of Cu nanoparticles, and $R$ values could be increased by increasing [TBAOH] under a fixed amount of $Cu(EH)_2$. A wider controllable range of $R$ values from 2.0 to 3.8 was allowed by adjusting [TBAOH] (see Figure 3B). The LSPR peaks were blue-shifted from 585 to 565 nm by raising $R$ values from 2.0 to 3.0, and a further shift was not observed when $R$ is above 3.0. The intensity of LSPR peaks diminished noticeably by increasing $R$ up to 3.8, whereas the LSPR $\lambda_{max}$ was not shifted. Quite an excessive amount of TBAOH ($R$ = 4.7) renders eventually a plasmon peak extinct. In other words, Cu nanoparticles could not be formed dominantly at this point. In the hydrazine reduction of $Cu(OH)_2$, an excessive amount of hydroxide ions was inclined to favor the predominant production of $Cu_2O$ particles rather than Cu.[30] Moreover, the hydrazine reduction of CuO, whose production was detectable at high $R$ values, could be terminated to form only $Cu_2O$.[31] The hydrazine reduction of Cu(II) species when $R$ is higher than 3.8 may result in the production of $Cu_2O$. Note that a significant amount of CuO could be formed when the $R$ value was raised up to 3.8. The concentration of hydroxide ions plays a significant role in preparing Cu nanoparticles in the present synthesis via hydrazine reduction.

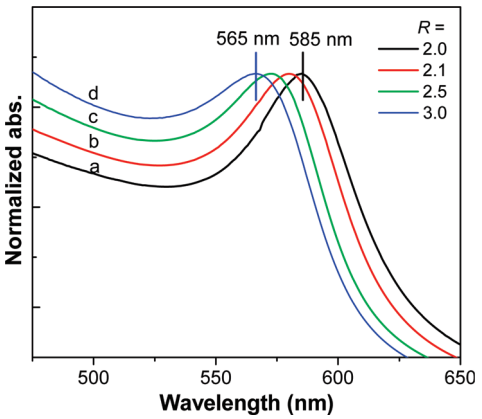


**Figure 4.** Normalized absorption spectra representing relative position and intensity of LSPR peaks. Spectrum (a) $R$ = 2.0, $\lambda_{max}$ = 585 nm; (b) $R$ = 2.1, $\lambda_{max}$ = 580 nm; (c) $R$ = 2.5, $\lambda_{max}$ = 573 nm; (d) $R$ = 3.0, $\lambda_{max}$ = 565 nm.

**Change in LSPRs with Geometric Variation of Cu Nanoparticles by Regulating *R* Values.** In Figure 4, absorption spectra measured with different $R$ values were relatively represented by the normalization at the $\lambda_{max}$. It was confirmed that the spectral shift of LSPRs due to increasing [TBAOH] parallels the change of LSPRs observed by decreasing [$Cu(EH)_2$] with respect to the spectral blue-shift of LSPRs occurring with an increase in the $R$ values. Only the $R$ values from 2.0 to 3.0, where the major production of Cu nanoparticles were expected, were selected to discuss the dependence of LSPRs on $R$ values. The gradual red-shift from 565 to 585 nm and relative spectral enhancement of LSPR peaks were manifest through the normalization as the $R$ value decreased from 3.0 to 2.0. The most intense peak centered at 585 nm emerged when $R$ = 2.0. A sequential decrease in relative intensity of LSPR peaks was observed with increasing the $R$ value, and it is obvious that the LSPRs were highly sensitive to the $R$ values.

To confirm correlation of nanoparticle geometries with corresponding LSPRs, the geometric characterization of Cu nanoparticles prepared at different $R$ values from 2.0 to 3.0 was conducted using electron microscopy.

(30) Xu, H.; Wang, W.; Zhu, W. *J. Phys. Chem. B* **2006**, *110*, 13829–13834.
(31) Wang, W.; Wang, G.; Wang, X.; Zhan, Y.; Liu, Y.; Zheng, C. *Adv. Mater.* **2002**, *14*, 67–69.

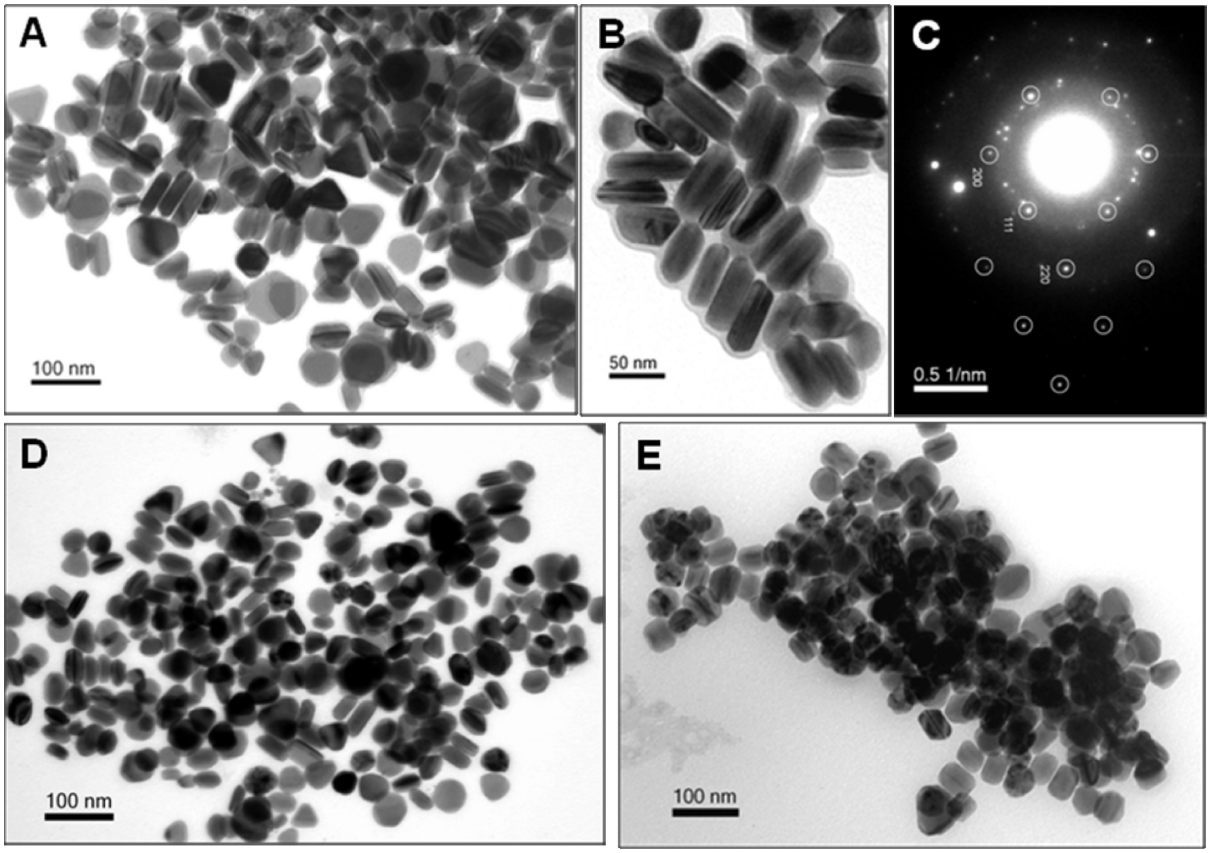


**Figure 5.** Corresponding TEM images showing geometries of Cu nanoparticles prepared at different $R$ values and an electron diffraction pattern of truncated Cu nanoplates. ((A, B) $R = 2.0$, corresponding LSPR $\lambda_{max} = 585$ nm; (C) electron diffraction pattern taken from the sample prepared at $R = 2.0$; (D) $R = 2.5$, LSPR $\lambda_{max} = 573$ nm; (E) $R = 3.0$, LSPR $\lambda_{max} = 565$ nm).

The Cu nanoparticles responsible for the most red-shifted and intense LSPRs at 585 nm were revealed to be composed of truncated triangular plates (45%), elongated particles (39%), and irregular particles (16%) as shown in Figure 5A. The existence of partial stacking of truncated Cu nanoplates along basal planes was also observed in the whole Cu colloid as represented in a magnified view of Cu particles (Figure 5B). Analogous partial stacking between neighboring nanoplates was also observed from relatively thick truncated Ag nanoplates.[32] The majority of the elongated Cu particles may be categorized as nanoplates in consideration of their perpendicular alignment. Truncated triangular nanoplates were indexed to be face-centered cubic Cu nanocrystals, as revealed by a SAED pattern (Figure 5C). The *d*-spacing values taken from most of diffracted spots are 0.211, 0.182, 0.128, and 0.110 nm, and close to lattice parameters for bulk Cu. The SAED pattern contains [011] zone axis diffracted spots of Cu, which are denoted with circles. There are a few spots with a *d*-spacing value of 0.215 nm, which corresponds to a (200) lattice plane of $Cu_2O$. The $Cu_2O$ appears to be formed on exposure to air during drying on grids. The average size of truncated triangular Cu nanoplates was estimated by TEM images, using more than 400 particles, and the thickness was taken from the stacked particles. Their size measured 60 nm ±15.3% in width of base and 22 nm ±12.5% in thickness, and almost all the basal planes of truncated triangular nanoplates are estimated below 65 nm in width. Irregular particles including distorted cubes and ellipsoids were generated below 16% of a whole colloid.

Cu nanoparticles prepared at $R = 2.5$ are shown in Figure 5D, and the corresponding LSPR $\lambda_{max}$ of the nanoparticles was blue-shifted to 573 nm (spectrum c in Figure 4). The TEM images of the nanoparticles show that the resulting morphologies are distorted, becoming disk-like and irregular with the shrinkage of size to around 50 nm in width. It is noteworthy that triangular and elongated geometries were maintained to some extent until the $R$ was raised up to 2.1 (see the Supporting Information, S1), whereas the production of ellipsoids and irregular particles losing truncated triangular geometries was clearly evident when $R$ was increased above 2.1.

When $R$ was further raised up to 3.0, the most isotropic geometries such as cubelike structures and spheres were found. The obtained Cu nanoparticles displayed the LSPR peak center at 565 nm. A further decrease in size, however, was not found, and the cubes and spherical particles were of a comparable average volume, measuring about 49 nm in diameter. The relative intensity in the LSPR taken from the nanoparticles obtained with given the highest $R$ value was dramatically diminished compared to LSPR intensity taken from most anisotropic particles prepared at $R = 2.0$.

(32) Zhu, J.; Bi, H.; Wang, Y.; Wang, X.; Yang, X.; Lu, L. *Mater. Lett.* **2008**, *62*, 2081–2083.

From the geometric analysis, it is clear that the increase in $R$ values results in a significant geometric variation of Cu nanoparticles. The optimum aspect ratio of Cu nanoparticles was attained when $R$ approached 2, which is the lowest value allowed in the present synthesis. We can also clarify the remarkable dependence of LSPRs on nanoparticle geometries by correlating optical spectra with corresponding geometries. The spectral red-shift of dipolar plasmon resonance peaks of anisotropic noble metallic nanoparticles such as nanoplates and nanoprisms is closely associated with an increase in aspect ratios, which are determined by the extent of anisotropic growth.[33−35] In addition, in the case of nanostructured Cu, such a red-shift of LSPR peaks was found from anisotropic nanoparticle arrays with increasing aspect ratios.[14] The sequential red-shift is likely to be a reflection of the increase in aspect ratios through the geometric control of Cu nanoparticles with decreasing $R$ values.

In particular, the absorption profiles taken with $R$ = 3.0 exhibit weak LSPR peaks and an increasing absorption curve below them as shown in Figures 3 and 4, unlike absorption spectra taken from truncated triangular nanoplates obtained at $R$ = 2.0 which show represent intense LSPRs and relatively low shoulders. In addition, an important aspect is the relative spectral enhancement of LSPRs along with the spectral shift. It is well-known that Cu has a dielectric function which is subject to the interband transitions extending to lower energy (∼2.15 eV) compared to those of Au and Ag.[36,37] Significant damping of LSPRs centered at 565 nm occurred, and the intensity of plasmon resonances diminished gradually as LSPR $\lambda_{max}$ approached the interband transition threshold below ∼577 nm.[37] The LSPRs of Cu nanoparticles obtained at $R$ above 2.5 were located within the interband transition region. In the present results, the relative enhancement of LSPR peaks could be observed by getting out of the interband absorption threshold through the spectral red-shift of LSPR $\lambda_{max}$ with increasing nanoparticle aspect ratios. The broad shoulders of the optical profiles are likely to originate from the interband transition absorption itself.[14,29] Very similar optical profiles of partially anisotropic Cu nanoparticles[28] and nanoplates[29] prepared with amphiphilic polymer stabilizers were found to show intense LSPR peaks. But the relative intensities of LSPRs taken from two different anisotropic nanoparticles are not quite identical. More intenses LSPR peaks were observed from the Cu nanoplates, due to their higher aspect ratios.

It is interesting to note that the anisotropic geometries, truncated triangular nanoplates, were induced just by adjusting the reactant concentrations such as [$Cu(EH)_2$] and [TBAOH] in nonionic microemulsion synthesis, in contrast to only a spherical geometry obtained in typical nonionic microemulsion methods.[27,38] Spherical noble metallic particles have been favored in the presence of symmetrical TBA halides,[39,40] short carboxylates,[41] and polyoxoanions,[42] whereas the anisotropic growth into plates and prisms have been found by asymmetrical tetraalkylammonium salts, such as cetyltrimethylammonium bromides which tend to form micelles in aqueous phase.[33,35] An excessive amount of TBA halides appears to have a detrimental effect on the anisotropic control of geometries in the present synthesis (see the Supporting Information, S2 and S3). Even a small amount of additional TBA halide salts, such as TBA chloride and bromide, caused a blue-shift of LSPRs even though $R$ was fixed at 2.0.

It should be recalled that the solubility of alkyl carboxylates was significantly raised by the cationic exchange with $TBA^+$ ions, and the phase behavior of micellar or vesicular solutions was exhibited through the association of the two opposite ions through the cationic exchange.[17−19] Therefore, from our investigation of the spectral change caused by additional counterions including halides and hydroxides, we suggest that the stabilization of anisotropic growth can be driven by the ion pairs of $TBA^+$ and ethyl hexanoates in water phases. $TBA^+$ salts have been also known to have a strong tendency to be adsorbed on the surface of noble metals.[39−42] In the present synthesis, the optimum condition for the control of truncated triangular geometries is found at $R$ = 2.0 where the ratio of [$TBA^+$]/[ethyl hexanoate] closely approaches 1.

As distinct from our previous results by tetraethylammonium hydroxide, present results show the remarkable susceptibility of nanoparticle geometries and LSPRs to the concentration of TBAOH.

**Truncated Triangular Cu Nanoplates in Different Nonionic Microemulsions.** The present synthesis of truncated triangular nanoplates was conducted by utilizing nonionic microemulsions emulsified by a NP-9 surfactant as one of polyoxyethylene (POE) nonyl phenyl ethers. Manipulation of size and corresponding optical response was attempted simply by altering the type of nonionic surfactants. As alternatives, NP-5 and NP-12 surfactants, which differ only in the length of POE blocks from NP-9 surfactants, were adopted. By processing the controlled reactions to yield truncated triangular nanoplates in NP-9 microemulsions, the effect of different $R$ values on resulting geometry and LSPRs of Cu particles were also examined in NP-5 and NP-12 microemulsions. As in the previous observations by using NP-9, the LSPRs of Cu nanoparticles were red-shifted on decreasing $R$ values in the two microemulsions, and optimum aspect ratios of anisotropic particles were achieved when $R$ = 2.0.

(33) Chen, S.; Carroll, D. L. *J. Phys. Chem. B* **2004**, *108*, 5500–5506.
(34) Ha, T. H.; Koo, H. J.; Chung, B. H. *J. Phys. Chem. C* **2007**, *111*, 1123–1130.
(35) Washio, I.; Xiong, Y.; Yin, Y.; Xia, Y. *Adv. Mater.* **2006**, *18*, 1745–1749.
(36) Ehrenreich, H.; Philipp, H. R. *Phys. Rev.* **1962**, *128*, 1622–1629.
(37) Rosei, R.; Lynch, D. W. *Phys. Rev. B* **1972**, *5*, 3883–3894.
(38) Qi, L.; Ma, J.; Shen, J. *J. Colloid Interface Sci.* **1997**, *186*, 498–500.
(39) Kolb, U.; Quaiser, S. A.; Winter, M.; Reetz, M. T. *Chem. Mater.* **1996**, *8*, 1889–1894.
(40) Rodríguez-Vázquez, M. J.; Blanco, M. C.; Lourido, R.; Vázquez-Vázquez, C.; Pastor, E.; Planes, G. A.; Rivas, J.; López-Quintela, M. A. *Langmuir* **2008**, *24*, 12690–12694.
(41) Rodríguez-Sáchez, M. L.; Rodríguez, M. J.; Blanco, M. C.; Rivas, J.; López-Quintela, M. A. *J. Phys. Chem. B* **2005**, *109*, 1183–1191.
(42) Watzky, M. A.; Finke, R. G. *J. Am. Chem. Soc.* **1997**, *119*, 10382–10400.

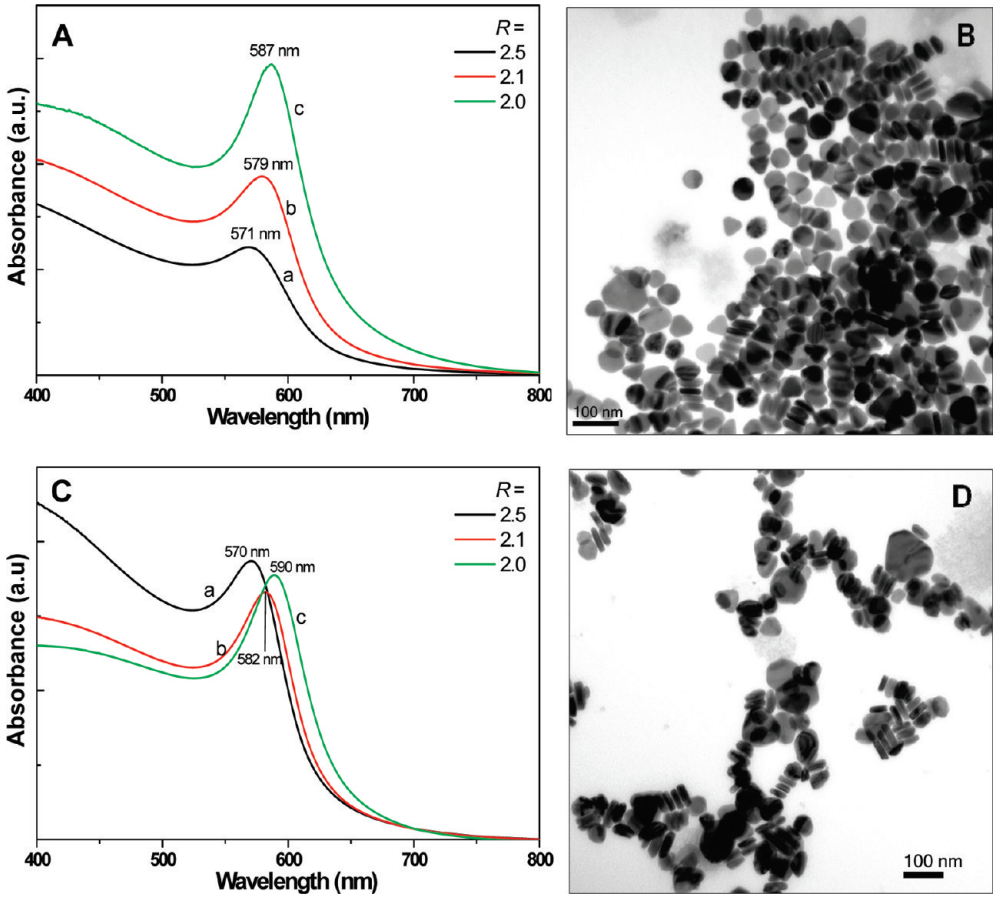


**Figure 6.** Absorption spectra of Cu nanoparticles prepared at different $R$ values in (A) NP-5 and (C) NP-12 microemulsions, respectively. (B, D) Corresponding TEM images of truncated triangular nanoplates prepared when $R = 2.0$ in the two microemulsion. The figures indicate LSPR $\lambda_{max}$ of each spectrum.

The results in Figure 6 also support the fact that truncated nanoplates are responsible for intense plasmon resonances. Absorption profiles showed the well-defined LSPR peaks and broad shoulders in common, and relative increase in the intensity of LSPRs was also observed along with spectral red-shifts as $R$ values approach 2.0.

Figure 6B represents geometries of Cu nanoparticles prepared in NP-5 microemulsions. The most abundant geometry of Cu nanoparticles is found to be truncated triangular plates (62%), and there are a minor amount of hexagonal plates up to 21% and stacked elongated particles (9%) together. Note that the formation of non-controlled ellipsoidal particles and irregular particles was almost excluded, amounts are below 8%. It is obvious on the basis of geometric analysis that the most effective anisotropic control of Cu nanoparticle geometries into truncated nanoplates was carried out in NP-5 microemulsions. Considering elongated structures as plates aligned perpendicular to substrates, the occupancy of nanoplates was over 90%. The size of truncated triangular nanoplates was measured to be 50 nm ±12% in width of basal planes, and hexagonal particles measured 47 nm ±8%. Thickness was estimated from elongated particles to be 17 nm ±12% on the assumption that elongated particles would be stacked nanoplates. Interestingly, the $\lambda_{max}$ of a LSPR recorded from truncated triangular nanoplates in a NP-5 microemulsion is located at longer wavelength (587 nm) than that of truncated triangular nanoplates obtained in a NP-9, even though the average size is below 50 nm in width and is smaller than truncated triangular nanoplates with a LSPR $\lambda_{max}$ of 585 nm. The longer wavelength appears to be attributed to the relatively narrow thickness of the truncated triangular nanoplates compared to their width. The aspect ratio, defined as the ratio of width to thickness, of truncated triangular nanoplates in NP-5 truncated triangular nanoplates is 2.9, which is higher than 2.7 of truncated triangular nanoplates prepared in NP-9 microemulsions. Similarly, nanoplates exhibiting hexagonal and truncated triangular geometries were obtained in a NP-12 microemulsion when $R = 2.0$, and the most red-shifted LSPR peak centered at 590 nm (Figure 6C and D). The nanoplates prepared in NP-12 microemulsions have the largest average size, 71 nm in width, with quite a large distribution, and their aspect ratio of 3.2 is the highest among three different truncated nanoplates, whereas the thickness of 22 nm is close to that of truncated nanoplates in a NP-9 microemulsion.

The truncated triangular nanoplates with different size ranges were synthesized through the same reactions only by altering the type of nonionic surfactant. The average size was confined in nonionic microemulsions to around 50 nm with NP-5 (HLB: 10), 60 nm with NP-9 (12.9), and finally 70 nm with NP-12 (14) in order. In the present

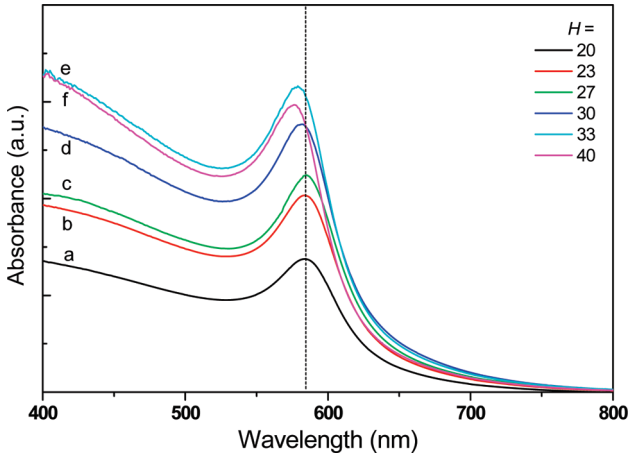


**Figure 7.** Effect of $N_2H_4$ concentration on absorption spectra of Cu nanoparticles. (a) $H = 20$, LSPR $\lambda_{max} = 584$ nm; (b) $H = 23$, $\lambda_{max} = 585$ nm; (c) $H = 27$, $\lambda_{max} = 585$ nm; (d) $H = 30$, $\lambda_{max} = 582$ nm; (e) $H = 33$, $\lambda_{max} = 578$ nm; (f) $H = 40$, $\lambda_{max} = 576$ nm.

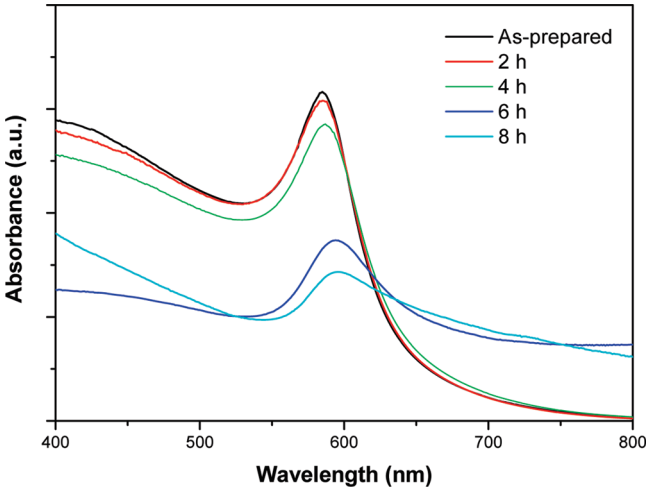


**Figure 8.** Temporal absorption spectra of Cu nanoparticles incubated on exposure to air under ambient condition. Each a spectrum was recorded from colloidal samples after different periods of exposure. Maximum wavelengths of absorption peaks during the oxidation are 585 (2 h), 587 (4 h), 594 (6 h), and 596 nm (8 h), respectively.

synthesis, results reveal that water phases stabilized by different POE blocks of nonionic surfactants influence the resulting size of nanoplates, and a trend that indicates the size of nanoplates increased as the length of hydrophilic chains increased is found in three different Cu nanoplates, although the effect of *n*-hexyl alcohol as cosurfactant cannot be fully understood in NP-12 microemulsions where the use of NP-12 should be required. The red-shifts of LSPR $\lambda_{max}$ to 587 and 590 nm were observed from truncated nanoplates prepared in NP-5 and NP-12 microemulsions, respectively.

The extent of spectral red-shifts may be closely involved with the optimum nanoparticle aspect ratios attained in three different nonionic microemulsions. The geometrical distribution can also be a likely factor affecting LSPRs, because there is a distribution of geometries from hexagon to triangular plates. Although all aspects of geometric differences in truncated nanoplates prepared in three different microemulsions cannot be completely taken into account, it is obvious that the most intense LSPR peaks emerged from the most anisotropic truncated triangular nanoplates, and the truncated plate geometries could be driven in the presence of $TBA^+$ ions and alkyl carboxylate anions regardless of the type of nonionic microemulsions.

**Effect of Reducing Agent Concentration.** The reduction of Cu(II) into Cu(0) was conducted by hydrazine in the water phase, and nucleation and growth took place in a single reduction step for the synthesis of Cu truncated triangular nanoplates. The effect of hydrazine was also examined by varying its amount in a fixed volume of water phases when $R = 2.0$. The $H$ value is defined as the molar ratio of $[N_2H_4]$ to $[Cu(EH)_2]$. As the $H$ value increased up to 27, the same amount of hydrazine in the experiments as discussed in the previous section, the intensity of LSPR peaks increased continuously, as shown in Figure 7. The enhancement of LSPR intensity appears to attribute to the increase in the amount of truncated triangular nanoplates after the same period of time. The peak when $H = 20$ displayed its LSPR $\lambda_{max}$ at 584 nm, but there was not a remarkable difference in the $\lambda_{max}$. The $[N_2H_4]$ should be raised to much higher concentration than $[Cu(EH)_2]$ not only to prevent the surface oxidation of Cu truncated triangular nanoplates under air atmosphere but to maintain the reduction rate sufficiently high enough to cover the whole growth stages. But the high reduction rate does not necessarily ensure the efficient anisotropic growth of Cu particles. In contrast to the results up to $H = 27$, LSPR peaks were shifted to blue when $H$ values were higher than 30 (582 nm), and the maximum position of a LSPR reached 576 nm with $H = 40$. The change in absorption spectra with varying $H$ values is not significant, but it represents a very similar trend to one under the control of the $R$ values. Despite using effective stabilizers, the anisotropic growth could not be induced efficiently when the reduction rates were too fast. A significant amount of disklike particles and spheres were produced at the high $H$ value (see the Supporting Information, S4). The efficiently slow reduction rate at the growth stage have been elucidated as a key to the anisotropic growth of metallic nanoparticles in a single reduction step.[33,41] In nonionic microemulsions, the growth stages went through the interdroplet dynamic exchange, so the reduction rate both relatively fast enough to facilitate the formation of Cu nanoparticles and slow enough to induce efficient anisotropic growth was required to avoid the production of roughly controlled Cu nanoparticles.

**Oxidation of Anisotropic Cu Nanoparticles on Exposure to Air.** Measurements of optical spectra and geometries in previous sections were made with colloidal Cu nanoparticles prepared in sealed vials containing constant volume of air. Particularly, optical measurements in the present work were carried out 8 h after initiation of hydrazine reduction of Cu(II) species. To examine the effect of oxidation on the LSPRs of Cu nanoparticles prepared at $R = 2.0$, we incubated as-prepared truncated Cu nanoplates on exposure to air by opening sealed vials,

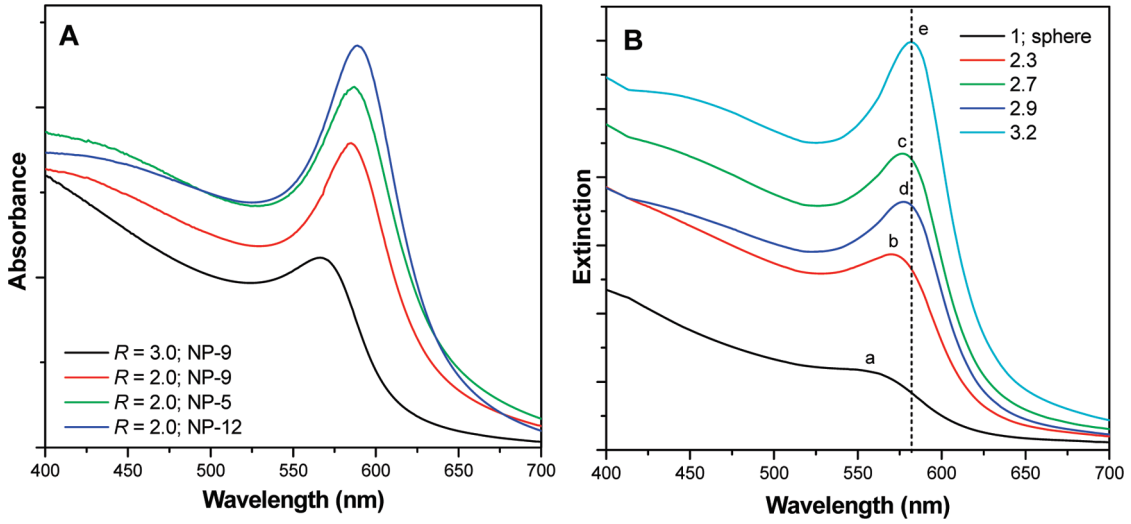


**Figure 9.** Comparison between experimental and calculated optical spectra of Cu nanoparticles. (A) Experimental absorption spectra of truncated Cu nanoplates obtained at $R = 2.0$ and nanoparticles obtained at $R = 3.0$. (B) Calculated extinction spectra of (a) a spherical target and (b−e) hexagonal prism targets with different aspect ratios. The aspect ratio of hexagonal plates is defined as width between two parallel edges of hexagon to thickness.

and a change in optical response of the Cu nanoplates was monitored at different periods of exposure time. We have already found in the present synthesis of Cu nanoplates that the concentration of hydrazine should be adjusted to the level where a reducing rate is high enough to overcome the oxidation rate regulated by air contained in closed glassware. The oxidation power of air appears to surpass the reducing power of a fixed amount of hydrazine when microemulsions containing anisotropic Cu nanoparticles are kept continuously exposed to air.

In Figure 8, a temporal change in optical spectra of anisotropic Cu nanoparticles on exposure air is illustrated. Even until after 2 h, a LSPR $\lambda_{max}$ was maintained at 585 nm, which is the same as that of as-prepared Cu nanoplates. A LSPR at this point also showed a well-defined peak. Although a slight spectral change, a red-shift of LSPR $\lambda_{max}$ to 587 nm and a small decline in LSPR intensity, occurred 4 h after initiation of exposure to air, there was not a manifest variation in line shape taken from the sample at this point. The absorption spectra still displayed narrow LSPR peaks. The rapid oxidation of Cu nanoparticles appears to be substantially inhibited by the remaining amount of hydrazine on completion of Cu(II) into Cu(0) until after about 4 h of exposure. A spectral shift and change in line shape were significant after 6 h. An LSPR shift to 594 nm was measured, with spectral broadening. The intensity of LSPRs diminished remarkably whereas broad absorption above 650 nm increased, altering the line shape of absorption spectra. The change of optical spectra continued until a colloidal sample started losing its colloidal stability 10 h after being left on exposure to air. The gradual oxidation of anisotropic Cu nanoparticles eventually gave rise to a significant dampening of a LSPR and just a broad absorption band extending from 450 to 800 nm after 8 h.

The temporal change of LSPRs during the oxidation of anisotropic Cu nanoparticles features a gradual red-shift and spectral broadening. The observed trend in the spectral change is an inverse trend in a change of experimental optical spectra measured during oxide shell removal of Cu nanoparticles surrounded by $Cu_2O$.[14] A similar trend of LSPR variation including damping and spectral broadening by the oxidation of poly(vinyl pyrrolidone)-capped Cu nanoplates was found in previous literature.[29]

**Simulated Extinction Spectra of Cu Nanoplates.** For a reasonable elucidation on the spectral change by increasing aspect ratios, electrodynamics calculations were carried out assuming representative geometries as hexagonal plates. It is not easy to take into account all the structural factors affecting the optical response of Cu nanoparticles, thus target geometries are simply assumed to be isotropic spheres and anisotropic hexagonal nanoplates for evaluating the effect of an increase in aspect ratios on dipolar plasmon resonances of Cu nanoparticles. All the extinction of Cu nanoparticles were calculated by using experimental average aspect ratios of Cu nanoparticles and dielectric constants of copper from Lynch and Hunter.[44]

Figure 9 illustrates a comparison between experimental and calculated extinction spectra of Cu nanoplates and isotropic Cu nanoparticles. A remarkable difference between line shapes of optical profiles recorded from the particles prepared at $R = 3.0$ and truncated triangular nanoplates at $R = 2.0$ prepared in three nonionic microemulsions. We have already speculated that the enhancement in intensity and spectral red-shifts of LSPR peaks is attributed to an increase in aspect ratios in Cu nanoparticles. Note that estimated aspect ratios from truncated nanoplates in NP-5, 9, and 12 microemulsions were 2.9, 2.7, and 3.2, respectively.

In Figure 9B, extinction spectra were calculated by taking into account the three aspect ratios of truncated

(43) Xiong, Y; McLellan, J. M.; Chen, J.; Yin, Y.; Li, Z. Y.; Xia, Y. *J. Am. Chem. Soc.* **2005**, *127*, 17118–17127.
(44) Lynch, D. W.; Hunter, W. R. In *Handbook of Optical Constants of Solids*; Palik, E. D., Ed. Academic Press: New York, 1985; pp 350−356.

triangular nanoplates prepared in different microemulsions. Extinction from sphere and prism targets with the aspect ratios of 1 and 2.3 was calculated additionally to evaluate the effect of the sequential increase in aspect ratios on the spectral change. Line shapes of extinction spectra calculated from the hexagonal plate targets are very close to those of absorption profiles consisting of intense plasmon resonance peaks and lower shoulders below them (spectrum c, d, and e). The hexagonal plate targets displayed the narrow and intense LSPR peaks in common, whereas the extinction spectrum of an anisotropic target with an aspect ratio of 2.3 and a sphere could not show any LSPR peak with a maximum. Moreover, in parallel to experimental results, the relative intensity of LSPRs increases gradually by raising the aspect ratios from 1.0 to 3.2, and the spectral red-shift from around 560 (spectrum a) to 582 nm (spectrum e) is also observed, although the intensity of a plate target with an aspect ratio of 2.9 is lower than a target with an aspect ratio of 2.7 due to the smaller particle volume of the geometric target.

The red-shifts and relative enhancement of LSPRs were also predicted from Cu spheroids by increasing geometric aspect ratios.[45] Line shapes exhibiting narrow LSPR peaks and flat shoulders below them are very close to those found in calculated extinction spectra of Cu nanodisks.[29] In the present calculations, we focused on the effect of aspect ratios on the changes in intensity and position of LSPRs. The predicted trend of spectral change with increasing aspect ratios from electrodynamics calculations indicates the evolution of intense LSPR peaks with their maximum at longer wavelengths, and is in agreement with the experimental trends.

## Conclusions

Anisotropic growth of Cu nanoparticles was attained by using Cu alkyl carboxylate salts and tetrabutylammonium hydroxide in nonionic microemulsions, and the resulting geometries were strongly influenced by the molar ratio of the two reactants. The optimum aspect ratios of Cu nanoparticles were attained with the molar ratio leading to the dominant production of copper hydroxide as intermediates. It was speculated and then demonstrated that geometric control of truncated triangular nanoplates can be induced by the use of ionic stabilizers of tetrabutylammonium alkyl carboxylate salts even in nonionic microemulsions. The same reactions using the identical ionic stabilizers led to the common production of truncated triangular nanoplates in three different nonionic microemulsions. The geometric control of truncated nanoplates could be carried out over 80% of the colloids in the present nonionic microemulsion syntheses, and especially, in NP-5 microemulsions, the proportion of Cu nanoplates was confirmed to be above 90%. Although there are slight geometric variations in nanoplates prepared in the three different microemulsions, it is revealed experimentally that optical spectra composed of narrow intense LSPR peaks and broad shoulders are observed from truncated Cu nanoplates with optimum aspect ratios through the geometric control. The strong dependence of LSPRs on geometric anisotropy is in agreement with the predicted trends taken from electrodynamics calculations. We conclude that the spectral red-shift accompanied with relative enhancement in the intensity of LSPR peaks is due to an increase in geometric anisotropy, and the observation of narrow and intense plasmon resonances can be ensured by geometric control of anisotropic truncated nanoplates.

**Acknowledgment.** This work was supported by the National Research Foundation grant funded by the Korea government (2009-0073777).

**Supporting Information Available:** A TEM image of Cu nanoparticles prepared when $R = 2.1$, UV−vis spectra of Cu nanoparticles prepared in the presence of additional amount of tetrabutylammonium halides, and a TEM image of Cu nanoparticles prepared at $H = 40$ are available (PDF). This material is available free of charge via the Internet at http://pubs.acs.org.

(45) Salzemann, C.; Lerm, J.; Urban, J.; Lisiecki, I. *Chem. Mater.* **2005**, *17*, 1279–1283.